Experiments on cold-formed steel moment-resisting connections with bolting friction-slip mechanism

Marzie Farnaz Shahini[a], Alireza Bagheri Sabbagh[a], Paul Davidson[a], Rasoul Mirghaderi[b], Shahabeddin Torabian[c]

[a] School of Engineering, University of Aberdeen, Scotland, UK, r01ms16@abdn.ac.uk

[b] School of Civil Engineering, University of Tehran, Tehran, Iran

[c] Senior Consulting Engineer, Simpson Gumpertz & Heger, Inc. Washington DC, storabian@sgh.com

[c] Associate Research Scientist, Department of Civil and Systems Engineering, Johns Hopkins University, Maryland, Baltimore, USA

Abstract

This paper presents an experimental investigation into the cyclic behaviour of cold-formed steel (CFS) moment-resisting (MR) beam-to-column connections utilising a friction-slip mechanism within a web-bolted connection arrangement. The bolting slip back and forth movements are accommodated through slotted holes to dissipate seismic energy within the CFS MR connections. Nine full-scale experiments were conducted on connections with and without slip for comparison purposes. The slip connections were designed to undergo slip prior to the initiation of local buckling in the CFS beam. This avoids premature local buckling, which could significantly degrade strength, particularly for connections with lower thickness beams. The slip connections, as a result, produce a greater energy dissipation capacity and ductility factor by up to 79% and 2.5 times, respectively, than that of the corresponding slip-resistant connections.

Keywords: Cold-formed steel; bolting friction-slip mechanism; seismic energy dissipation; moment-resisting connections.

1. Introduction

The primary lateral load resisting systems for the current best-practice lightweight steel framing (LSF) structures comprising cold-formed steel (CFS) walling stud and flooring joist sections are limited to tension-only strap-braced walls, integral wall bracing, wood-based or steel sheathed wall panels [1]. These systems, typically, suffer from significant pinching in their hysteretic response [1-3] leading to relatively low seismic energy dissipation capacity. A recently completed testing campaign on LSF floor-to-wall connections [4] showed premature local failure limit states due to an out-of-plane load transferring mechanism within the joist-to-stud connections. To address the identified limitations in stud-wall LSF systems a new semi-rigid floor-to-wall connection has been recently developed [5] providing an in-plane load transferring mechanism within the connection components. Sato and Uang

[6, 7] have developed a Special Bolted Moment Frames (SBMF) which features CFS channel beams directly bolted to both sides of hollow structural section columns satisfying the design requirements specified in AISI-S400-15 [8]. Within SBMF, the ductility capacity for seismic design is achieved through localised yielding in the bolted connection itself, rather than the sections' capacity. The reason is the relatively low local buckling resistance of typical CFS sections as the limiting moment capacity at the beam-column joints lesser than the yielding capacity. This study particularly highlighted bolt bearing as suitable ductile yielding mechanisms, but the application to multi-storey buildings is not considered.

A comprehensive investigation has been carried out by Bagheri Sabbagh et al. [9-12] on developing a new CFS moment-resisting (MR) beam-to-column connection to provide ductility and seismic energy dissipation capacity through beam yielding. Fig. 1 shows a schematic view of the developed CFS MR connection comprising a curved-flange beam section and a web-bolted through-plate (TP) connection stiffened by additional transverse plates welded inside the connection region. By means of full-scale connection tests and validated finite element (FE) modelling, it was demonstrated that local buckling resistance can be increased, and a relatively high ductility and energy dissipation capacity can be achieved through beam yielding. It was also found that activation of the bolting friction-slip mechanism, in addition to the beam yielding, can further improve the ductility and energy dissipation capacity of these connections satisfying the AISC Seismic Provision requirements [13] for Special Moment Connections. The proposed bolting friction-slip mechanism can be categorised as a seismic dissipative device with potential applications in other areas (e.g. in passive control systems [14]) that can be further explored in future research.

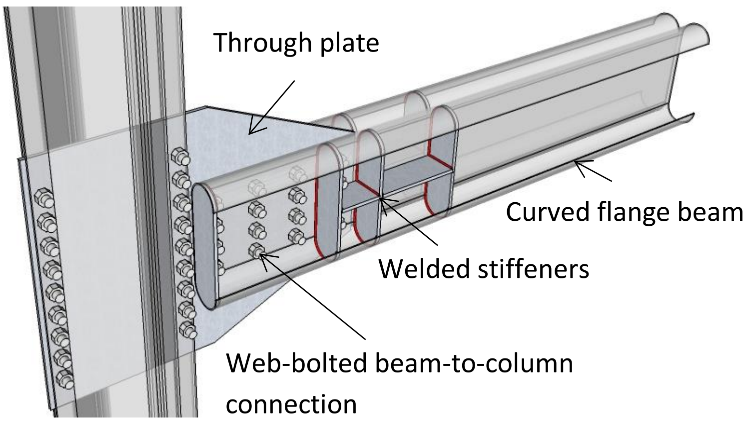

Fig 1. Schematic view of the developed CFS MR web-bolted connection.

Figs. 2 (a) and 2 (b) show the hysteretic moment-rotation responses for the connections dominated by beam local buckling and the bolting friction-slip mechanism, respectively. It can be observed that the latter type of connection produces a highly stable hysteretic response, while the former type of connection encounter strength degradation due to the occurrence of beam local buckling. Further FE and optimisation studies, on the same type of CFS MR connections, by other research groups [15] also demonstrated a relatively high level of ductility capacity through bearing action of the bolts within standard clearance bolt holes. More recently another type of CFS MR connection has been developed by Bagheri Sabbagh et al. [16], comprising beam and column built-up hollow sections infilled with rubberised concrete. Within this connection, the beam local buckling can be postponed through the restraining effect of the infilled material. As a result, a greater bending moment strength and energy dissipation capacity than those of the bare steel connections can be achieved [16].

To further explore the bolting friction-slip as the primary seismic energy dissipation mechanism of CFS MR connections, slotted bolting configuration has been studied by the authors [17-18] through a detailed FE investigation validated by experiments. Both square and circular bolting arrangements were considered incorporating a range of bolting slip moments within a parametric FE work [17-18]. Incorporation of bolting friction-slip, as the seismic energy dissipation mechanism, can facilitate the manufacturing process of such connections by eliminating the need for transverse stiffeners (shown in Fig. 1), adopted in previous studies [i.e., 9-12]. Further, the curved flange beam sections (shown in Fig. 1) can be replaced by segmental or folded flange beam sections in line with the ease of manufacturing approach. The choice of the slotted holes, arranged at a tangent to the bolts rotational motion under bending moment, was to overcome an existing limitation of the bolts with standard holes in energy absorption experienced only at the limits of travel of the bolts. By using slotted holes for the bolts, the bearing action is expected to be postponed, which consequently delays shifting the deformation/ductility demand to the beam and hence eliminates/delays local buckling. It was also revealed that the circular bolting arrangement provides a more uniform bolt force distribution than the corresponding square arrangement. Furthermore, it was found that the instantaneous centre of rotation of the slip connections is less deviated from the idealised centre of rotation than that of the connections without slip. These potentially lead to a more reliable connection design to postpone local buckling and therefore base the design of the full-scale connection tests presented herein. Other applications of slotted bolting connections could include attachment of exterior architectural façades to the main structure for seismic loading [19] which can be another topic for a future research.

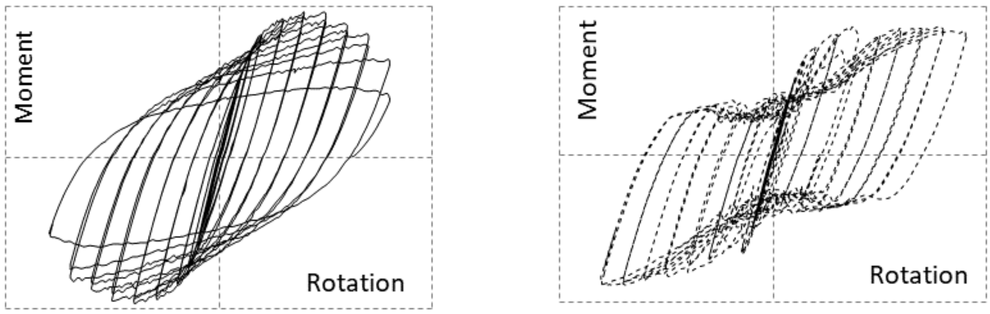

(a) Dominated by yielding and local buckling **(b)** Dominated by bolts friction-slip

Fig 2. Hysteretic responses of the developed CFS MR beam-to-column connections [9].

The design considerations of the test connections are first explained followed by the test set up, instrumentation, loading protocol, test observations and results.

2. Design considerations of the tested connections

Both slip and slip-resistant connections (labelled as SC and SRC, respectively) were tested for comparison purposes. Fig. 3 shows schematic views of the SC and SRC connection configurations comprising beam-to-TP circular bolting (CB) arrangement, with 50 mm length slotted holes on the TP, connected to a stub column through a bolted TP connection, passing between the beam and column channel sections. The beam channels were connected to one another using equally spaced filler plates to make a built-up section. The choice of CB was due to a more uniform bolt force distribution compared with that of the square bolting (SB) arrangement as discussed in the accompanying FE investigation reported in [18]. The length of the slotted holes was twice that of calculated in [18] to comfortably accommodate the back-and-forth travel of the bolts during the cyclic loading to delay the possible bearing action.

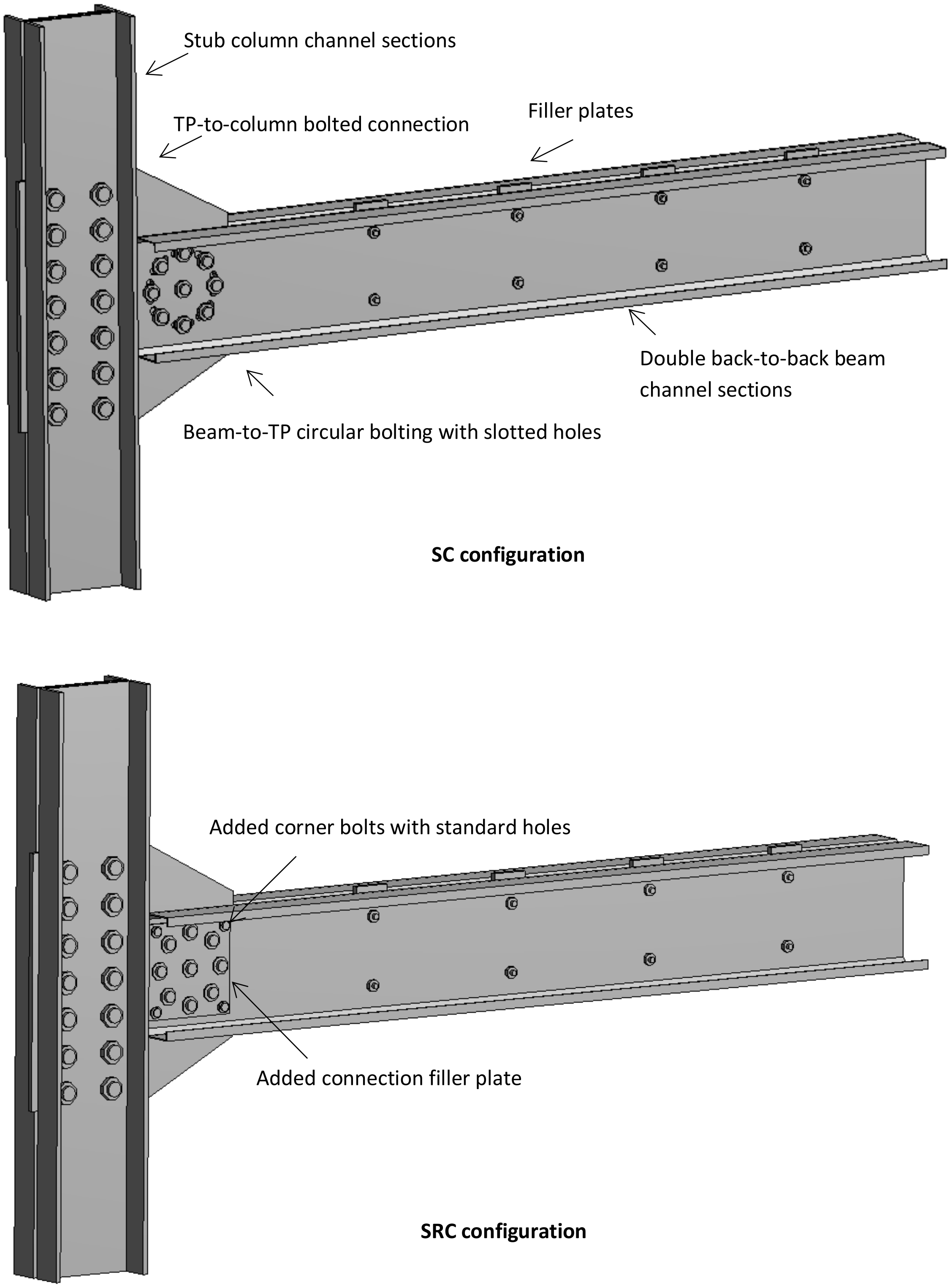

Fig 3. Schematic view of the SC and SRC connections using circular bolting arrangement.

The SC configuration was designed based on the beam-to-TP bolt group slip resistance value being less than the nominal bending moment strength of the beam, M_n, projected to the connection centroid. For the SRC configuration, four bolts with standard holes were added at the corners of the original circular bolt group to increase the level of the bolting friction-slip-grip resistance to be greater than the projected M_n to the connection centroid. All the SRC tests were conducted after the initial SC tests on the same specimens. To recover the initial bolting frictional resistance, a 2 mm thickness filler plate was added underneath the bolt nuts of the SRC connections. The friction-slip-grip actions of the bolts during the initial SC tests can be traced on the TP (with slotted holes) and the beam web plates (with standard holes) as shown in Fig. 4. It should be noted that this filler plate was also added to the SC connections with 2 mm thickness beam sections to postpone the premature beam web buckling (discussed under section 4.1).

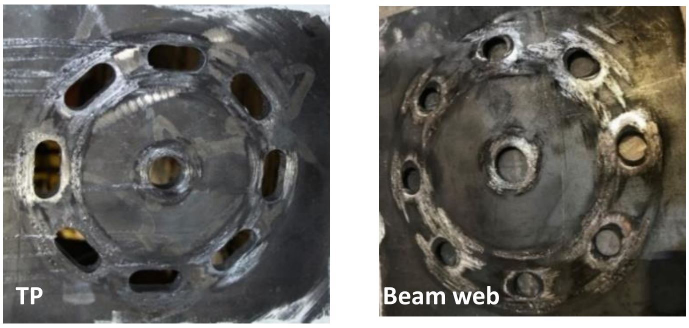

Fig. 4. Trace of the bolt friction-slip-grip action on the TP and the beam web plate during the SC tests.

Listed in Table 1 are nine SC or SRC testing connection configurations having two types of double back-to-back segmental- or flat-flange lipped channel beam sections (labelled as S or F, respectively) with a range of 2 mm, 4 mm, or 6 mm thicknesses. The channel sections, sketched in Table 1, had the overall dimensions of 300 mm web depth, 125 mm flange width and 25 mm edge lips. The S-flange sections had greater flange local buckling resistance than that of the corresponding F-flange sections chosen for comparison purposes.

Table 1. Tested connection configurations.

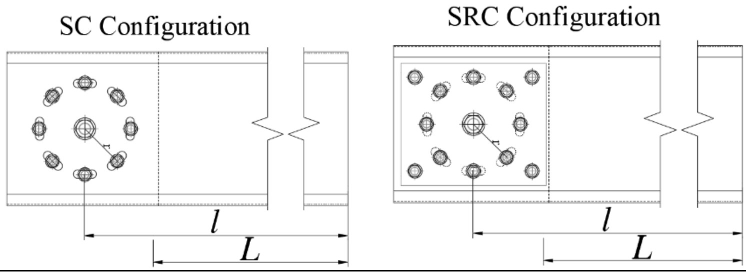

Test labels	Connection type	Segmental or flat-flange beam	Beam thickness	Bolting arrangement	Added connection filler plate
SC-S-2	Slip	Segmental	2 mm	Circular	√
SC-S-4	Slip	Segmental	4 mm	Circular	-
SC-S-6	Slip	Segmental	6 mm	Circular	-
SC-F-2	Slip	Flat	2 mm	Circular	√
SC-F-4	Slip	Flat	4 mm	Circular	-
SC-F-6	Slip	Flat	6 mm	Circular	-
SRC-S-2	Slip-resistant	Segmental	2 mm	Circular	√
SRC-S-4	Slip-resistant	Segmental	4 mm	Circular + 4 corner bolts	√
SRC-S-6	Slip-resistant	Segmental	6 mm	Circular + 4 corner bolts	√

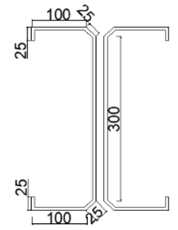

Segmental-flange

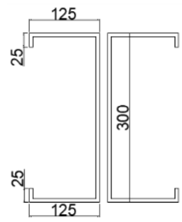

Flat-flange

The SC and SRC connections, with sketches in Table 1, were respectively designed to satisfy $M_{conn,SC} < l/L\ M_n/1.5$ and $M_{conn,SRC} > l/L\ M_n$, where l and L are the distances from the free end of the beam to the connection centroid and to the end of the through plate inside the beam, respectively. These design inequalities are related to the concepts discussed above to ensure the bolt group undergoes slip prior to the beam local buckling in SC, while the beam local buckling may, theoretically, precede the connection slip in SRC configurations. Incorporation of the safety factor of 1.5 in the SC inequality is aligned with the FE results reported in [18] accounting for the physical and design uncertainties. The nominal bending moment strength of the beams, M_n, were calculated using Direct Strength Method (DSM) design equations, prescribed in Appendix 1 of AISI S100 specifications [20]. The elastic buckling moments, accounting for local and distortional buckling, inputting into DSM, were determined using the CUFSM finite strip software [21]. All the steel sections and through plates had the steel grade of S275 with the nominal yielding strength of 275 MPa incorporated into the design equations herein.

High strength friction grip (HSFG) bolts with 10.9 grade of M16, M20 and M24 diameters were used for 2 mm, 4 mm, and 6 mm beam sections, respectively. The bolt group slip capacity of SC (see Fig. 3) having n = 8 bolts located at a radius of r = 100 mm, each with a slip capacity of F_{slip}, can be calculated as follows:

$$M_{\mathrm{conn,SC}} = n\, F_{\mathrm{slip}} \times r \qquad \text{(Eq. 1)}$$

where F_{slip} has been calculated as per section 3.9.1 of EN 1993-1-8 [22] assuming a friction coefficient of 0.3. In the same way $M_{\mathrm{conn,SRC}}$ can be calculated for SRC configuration having the additional 4 corner M16 bolts located at r = 160 mm.

The calculated values for $M_{\mathrm{conn,SC}}$, $l/L\ M_{\mathrm{n}}/1.5$, $M_{\mathrm{conn,SRC}}$, $l/L\ M_{\mathrm{n}}$, F_{slip} and the bolt pretension forces are given in Table 2. All the bolts were tightened to reach the pretension load specified in Table 2 using Skidmore Bolt Load Meters type of torque wrench. It is worth mentioning that a reduced slip coefficient of 0.19 [22] could be adopted (in lieu of the assumed 0.3 value) in case of a coated connection exposed to aggressive outdoor environmental conditions protected by e.g., a galvanised coating. As a result, a greater pretension force would be required to reach the same level of the slip resistance as that of the original design.

Table 2. Design information for the tested connection configurations.

Test labels	$M_{\mathrm{conn,SC}}$	$l/L\ M_{\mathrm{n}}/1.5$	$M_{\mathrm{conn,SRC}}$	$l/L\ M_{\mathrm{n}}$	F_{slip}	Bolt pretension force
	kN.m	kN.m	kN.m	kN.m	kN	kN
SC-S-2	28.6	30.6	-	-	38.2	56.9
SC-S-4	75.4	80.6	-	-	100.8	300
SC-S-6	118.9	127.1	-	-	158.9	472.8
SC-F-2	25.9	27.7	-	-	34.6	51.55
SC-F-4	68.6	73.3	-	-	91.6	272.7
SC-F-6	112.7	120.4	-	-	150.5	448
SRC-S-2	-	-	48.2	45.9	57.4	85.3
SRC-S-4	-	-	127.0	121.0	84.00	125
SRC-S-6	-	-	200.2	190.6	132.39	197

It should be noted that for the SRC configuration with 2 mm beam thickness the required slip resistance to satisfy the SRC design inequality was achieved solely by increasing the pretension forces of the bolts, thus no need for the additional corner bolts which were employed for the connections having 4 mm and 6 mm thickness beams. It should be mentioned that in design of the so called SRC connections it has been assumed that the frictional resistance of the slotted bolts has been fully recovered through the addition of the filler plates. However, the obtained results for the SRC connections, discussed under section 4.2, showed a level of slip within the connection prior to the beam local buckling. This reveals inadequate friction roughness between the connection plate surfaces.

The bolt located at the bolt group centroid had a standard hole and was merely used to tie the beam web and the TP avoiding a web buckling at the connection region. This also provides a constraining effect for a more uniform rotation of the perimeter bolts about the centre bolt as indicated in [18]. In the above calculations the centre of rotation has been assumed at the centroid of the bolt group. This assumption has been proven to be reasonably accurate up to a relatively large connection rotation at the inelastic region according to the initial FE work [18]. To ensure the TP remains elastic, a conservative thickness of 15 mm has been chosen, calculated based on the projected nominal beam moment capacity of M_n at the face of the column.

3. Testing arrangement

The SC and SRC testing specimens (listed in Table 1) were set up, instrumented and tested under cyclic loading. The beam flat-flange and segmental-flange sections of the tested connections were fabricated using a press brake through a sequential bending process at the corners of the predrilled steel sheets as shown in Fig. 5. The average yielding and ultimate strengths and elongation at rupture taken from the tensile coupon tests of the 2 mm, 4 mm and 6 mm thickness steel plates utilised for the beam sections are given in Table 3. As can be observed, the actual yield strengths are in good agreement with the nominal strength of the S275 steel grade assumed in the above design process.

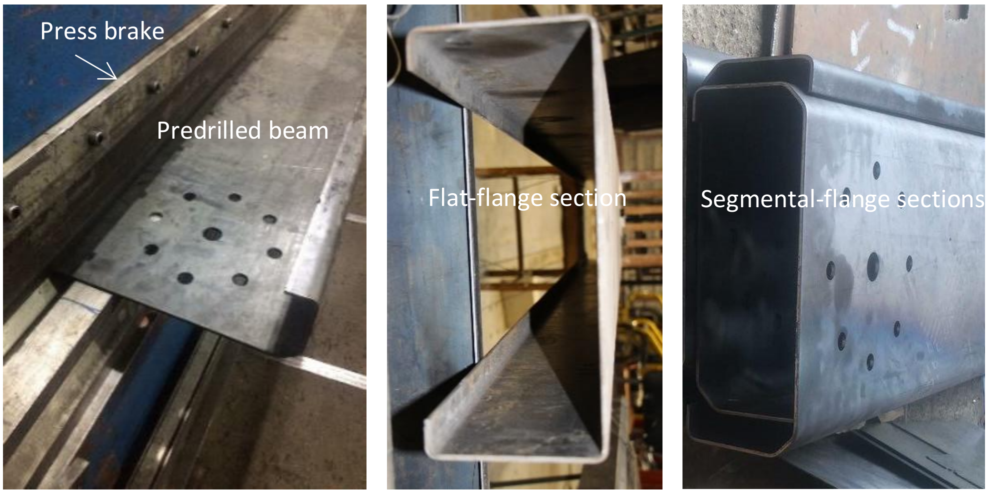

Fig 5. Fabrication of flat-flange and segmental-flange beam sections using press brake.

Table 3. Averaged test resuls for material properties

Plate thickness (mm)	Yielding strength (MPa)	Ultimate strength (MPa)	Elongation at rupture (%)
2	260.5	346	16.85
4	268	370.5	17.75
6	274	368	18.95

3.1. Test set-up

Fig. 6 shows a drawing and a photo of the test set-up comprising a vertically aligned testing specimen supported by heavy hot-rolled steel sections and a strong floor, loaded at the free end through loading actuators supported by a test rig. The testing beam was bolted to the double back-to-back hot-rolled steel channel sections (using M24 bolts) which served as the stub column for the tested connections. The distance between the centre of the loading point to the face of the stub column was 2500 mm representing inflection point of a 5000 mm span moment frame under lateral loading conditions. The lateral restraint is provided at the mid-length of the beam to prevent any out-of-plane movement and lateral-torsional buckling effects on the beam behaviour.

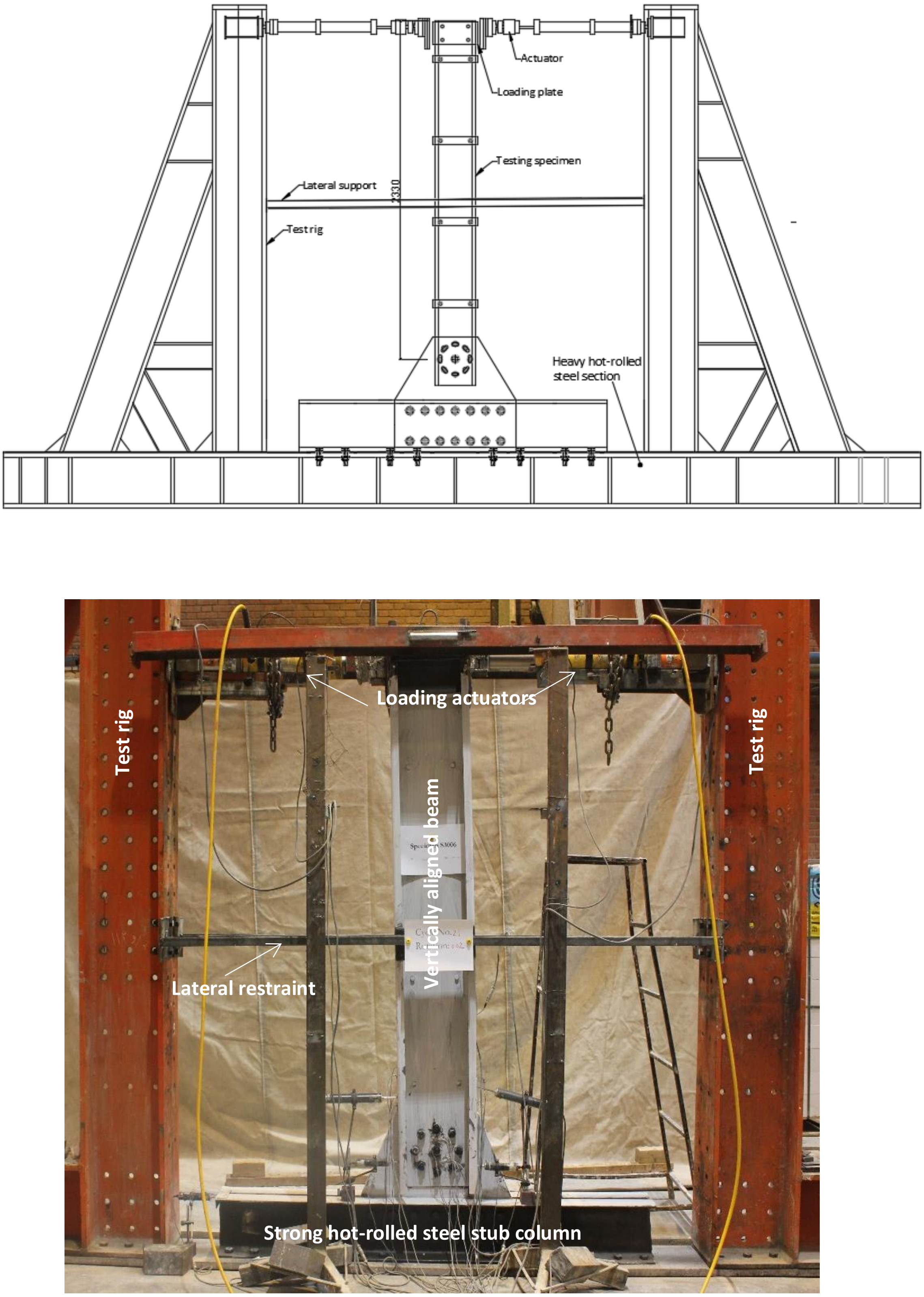

Fig. 6. Test set-up.

3.2. Loading protocol

Fig. 7 displays the AISC Seismic Provisions [11] cyclic loading protocol, determined based on the connection rotation of θ, which has been adopted for qualifying steel beam-to-column moment connections in special and intermediate moment frames (SMFs and IMFs). The distance between the loading point and the connection centre (2330 mm as shown in Fig. 6) has been used to determine the displacement of the actuator for a given value of connection rotation.

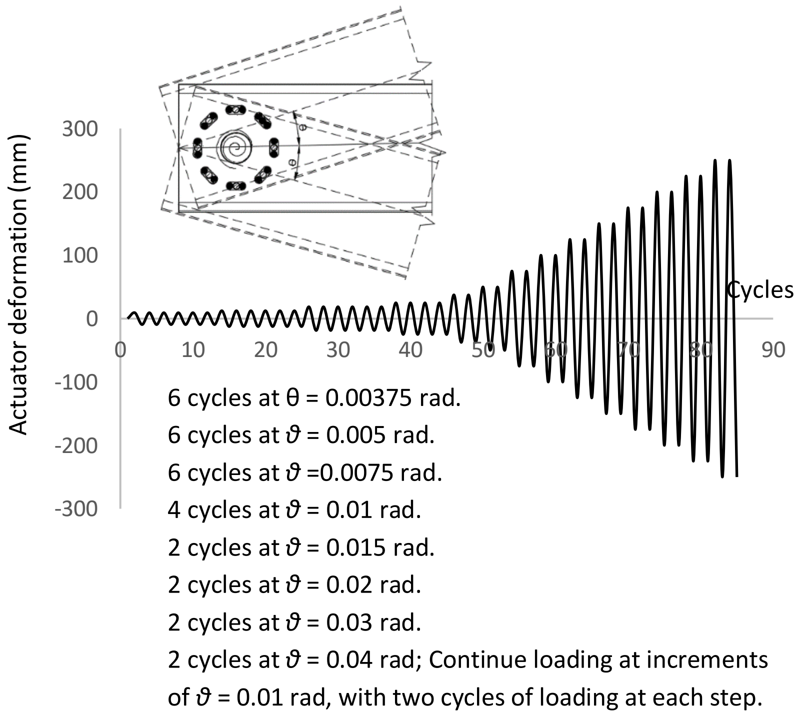

Fig. 7. Loading cycles.

3.3. Instrumentation

To measure the strains and deformations at the critical locations of the specimens, strain gauges (SGs) and displacement transducer were mounted, as shown in Fig. 8. SG01-SG04 were placed on the TP to ensure its elastic behaviour, while SG05-SG12 were attached on the beam flanges where local buckling was expected, particularly in SRC connections. Two displacement transducers of L01 and L02 were positioned at the end of the beam to measure the beam end displacements.

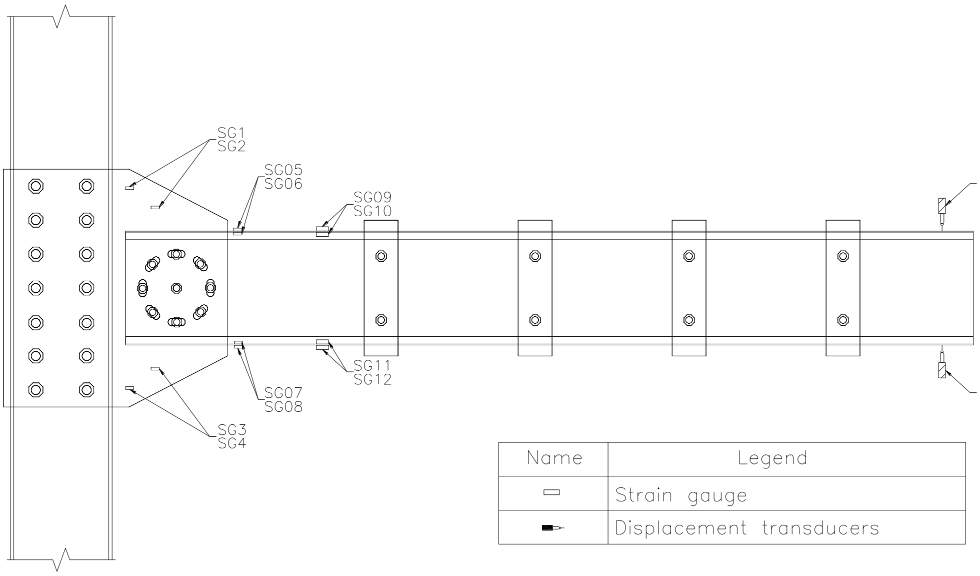

Fig. 8. Instrumentation sketch for the specimens.

4. Test results

The normalised moment-rotation (M/M_n-θ) curves, test observations and strain distribution results of the SC and SRC specimens, listed in Table 1, are presented in the following subsections. The beam bending moment, M, and rotation, θ, have been calculated at the connection bolt group centre which has been assumed as the main source of the connection ductility capacity particularly for the SC design.

4.1. SC specimens: connections dominated by bolt slip

Fig. 9 shows the M/M_n-θ curves of the SC-S (F)-2,4 and 6 specimens. Different regions can be identified as denoted by AB, BC and CD, respectively referring to the elastic, pre-buckling slip-grip (for all the connections) and post-buckling (for 2 mm connections only) regions. It should be noted that, given the bolted connection design and installation uncertainties, the pretension forces were applied in two stages ensuring slip would occur prior to the beam local buckling. Initially, a lower level of pretension forces than those specified in Table 2 was applied. This resulted in a hysteretic curve with a relatively lower stiffness pre-buckling region due to a low or no gripping action of the bolts travelling back and forth within the holes. The obtained hysteretic curves for the representative SC-S-4 and SC-S-6 specimens with a lower level of pretension forces have been shown by dotted lines in Fig. 9. Subsequently, the pretension force level has been increased to the maximum values specified in Table 2 which resulted in the hysteretic curves shown by solid lines.

As can be observed all the SC specimens produced a highly stable hysteretic behaviour and sustained 80% of the peak moment exceeding 0.04 rad rotation required for SMFs [11]. After the elastic cycles (region AB) the specimens with the higher level of pretension forces underwent the slip-grip region (BC) during which the connections produced a considerable level of stiffness up to point C. This could be due to an intermittent griping action of the bolts tightened with the maximum pretension forces. As a result of this action the deformation demand was partially shifted to the beam which could result in an undesirable beam local buckling followed by a strength degradation (CD), occurred in the connections having 2 mm thickness beam sections (i.e., SC-S (F)-2). As expected, the overall trend of the hysteretic responses for SC specimens are not considerably affected by the type of beam sections (i.e., S, or F sections).

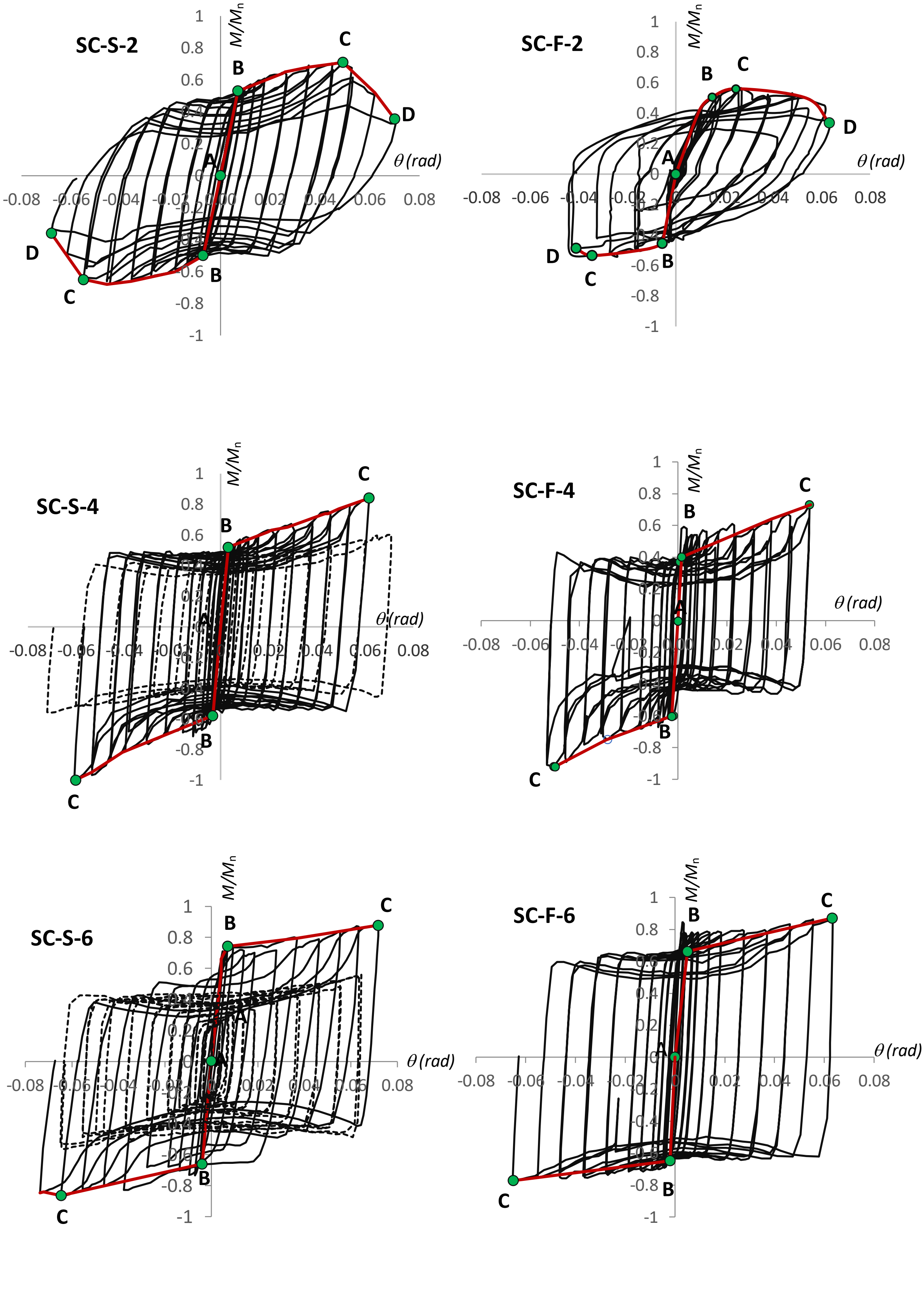

Fig 9. Hysteretic responses (M/M_n-θ curves) of the SC-S (F)- 2, 4 and 6 specimens with bolt pretentesion forces at the maximum or lower level than those specified in Table 2 (shown by solid or dotted lines, respectively).

4.1.1 *Test observations of specimens SC-S-2 and SC- F-2*

The strength degradation for the SC-S-2 specimen initiated at around θ = 0.05 rad with the peak moment of $0.7M_n$ (point C as shown in Fig. 9, SC-S-2) due to a web local buckling (WLB) which was intensified in the following cycles (see Fig. 10). This followed by a flange distortional buckling (FDB) and consequently failure of the specimen at around θ= 0.07 rad (i.e., point D in Fig. 9). For the SC-F-2 specimen, a similar hysteretic moment-rotation trend can be identified with a lower peak moment of $0.6M_n$ and a smaller area surrounded by the hysteretic curves. This indicates a lower energy dissipation capacity, as discussed under Section 5. Further, the WLB failure initiated at an earlier rotation of around 0.02 rad (shown by point C in Fig. 9, SC-F-2) compared with that of SC-S-2 specimen. This could be due to a higher stiffness provided to support the web plates by the segmental flanges compared with that of the flat flanges.

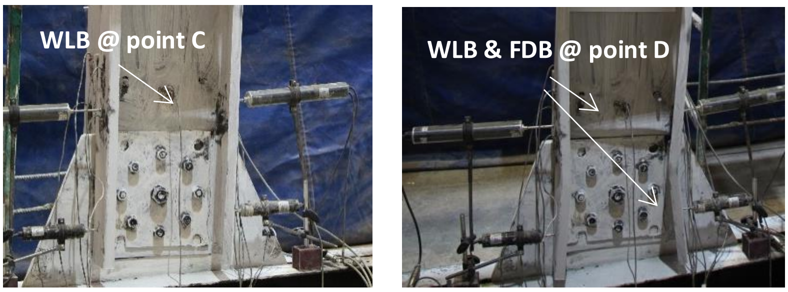

Fig 10. Web local buckling (WLB) and flange distortional buckling (FDB) in specimen SC-S-2 at CD region.

4.1.2 *Test observations of specimens SC-S (F)-4 and 6*

The SC specimens having higher beam thicknesses of 4 mm and 6 mm showed a bi-linear (AB-BC) behaviour with no strength degradation up to a very large rotation of around θ= 0.06-0.07 rad, as can be seen in Fig. 9. No trace of local buckling/failure was noted at point C, as can be observed in Fig. 11 for the representative SC-S-4 connection. This led to a relatively higher level of peak moment (compared with the 2 mm beam connections) reaching around 0.8-1.0 M_n.

3

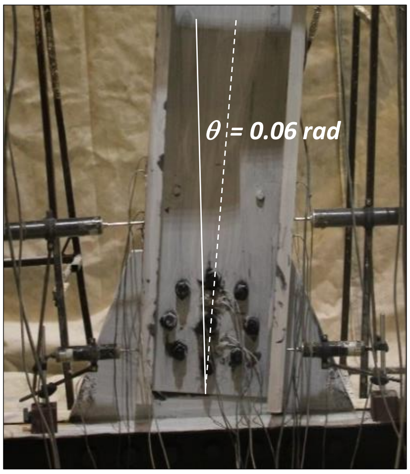

Fig 11. Specimen SC-S-4 with no trace of local buckling at 0.06 rad (point C).

4.2. SRC specimens: connections dominated by rotation in the beam

Fig. 12 shows the hysteretic curves for the SRC-S-2,4 and 6 specimens. In the same way as the SC specimens, different regions of AB, BC and CD can be identified. The main difference is that the BC region of the higher thickness beam specimens (i.e., SRC-S-4 and 6) shows a higher stiffness due to the addition of the four corner bolts with standard holes as discussed under the design considerations above. This led to the bearing action of the added bolts against the standard holes, thus a higher connection stiffness and strength than the SC counterparts were achived. The bearing action within the standard holes could occur in conjunction with the slip-grip action of the original bolts within the slotted holes. For the SRC-S-4 connection, however, two segments with different levels of connection stiffness can be identified within the BC region which are labelled as BC` and C`C. The reason being a possible delay of the bearing action of the four added bolts within the standard holes to be fully mobilised at around point C`. Compared with the SC specimens, a lower level of bolting frictional resistance was mobilised within the SRC bolting connections. This is attributed to the reduction of frictional roughness between the connection plate surfaces due to the slip-grip action that occurred during the initial SC tests (as evidenced in Fig. 4). This, therefore, indicates that the added filler plates have not fully recovered the initial frictional resistance, as assumed in the design of the SRC connections.

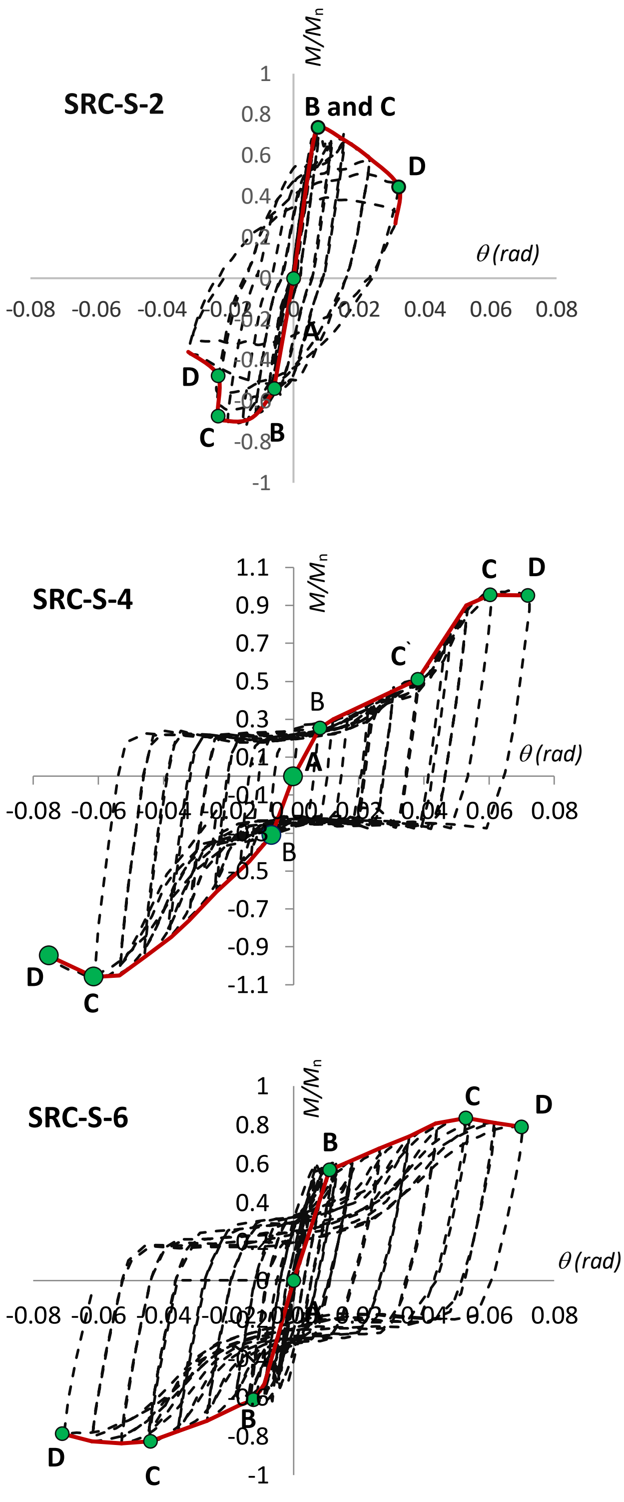

Fig 12. Hysteretic responses (M/M_n-θ curves) of the SRC-S- 2, 4 and 6 specimens.

4.2.1 Test observations of specimen SRC-S-2

As can be observed in Fig. 12, no slip occurs in the SRC-S-2 specimen which predominantly shifts the deformation demand from the connection into the beam. This led to a premature web local buckling (WLB, shown in Fig. 13) that occurred at θ = 0.0075 rad (point C in Fig. 12), reaching the peak moment of 0.74M_n. This was intensified and followed by a relatively sharp strength degradation reaching point D at around 0.032 rad due to a flange distortion buckling (FDB, shown in Fig. 13). No distinguishable BC region was noticed, in Fig. 12, for the positive SRC-S-2 cycles due to the premature WLB.

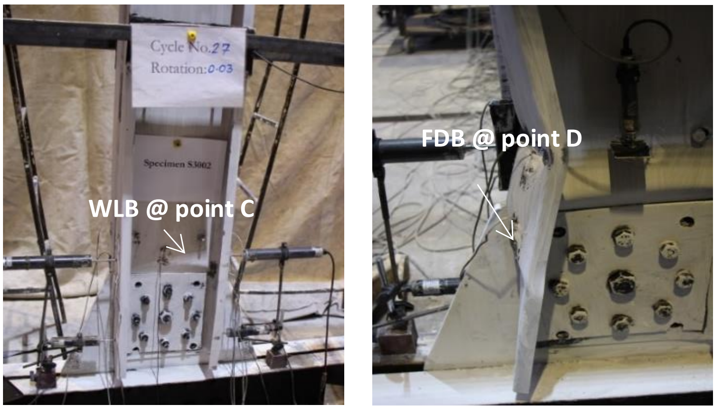

Fig 13. Web local buckling (WLB) and flange distortional buckling (FDB) in specimen SRC-S-2 at CD region.

4.2.2 Test observations of specimens SRC-S-4 and 6

By increasing the beam thickness to 4 mm and 6 mm, the local buckling failures were postponed to a larger rotation beyond the SMFs requirements, and the peak moment, corresponding to point C, reached the level of beam nominal moment of M_n. Both SRC-S-4 and 6 specimens experienced a strength degradation after point C which led to a slight drop to point D as shown in Fig. 12. This was due to a web local buckling initiated at point C which was intensified at point D reaching around θ = 0.07-0.08 rad (as shown in Fig. 14 for SRC-S-6).

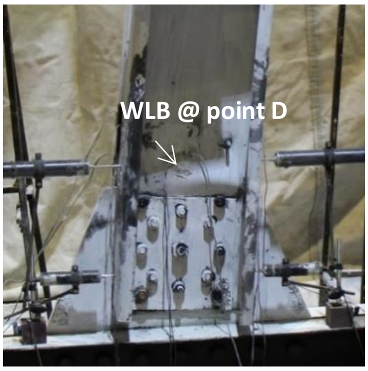

Fig 14. WLB at point D in specimen SRC-S-6.

4.3. Strain distributions

The maximum strain values normalised by the proof strains, ε_y = 0.2%, on the critical sections of the TP and the beam flanges, for the representative SC-S-4 and SRC-S-4 specimens are shown in Figs. 15 and 16, respectively. The peak strain values of the TP are around 0.31 ε_y which is well below the yielding strain; therefore, as expected, the TP remained elastic during the whole loading cycles for both the SC and SRC connections.

For the representative SC-S-4 specimen, the peak normalised strain values at the beam flanges (shown in Fig. 16) slightly exceeded unity for SG06-SG08. However, the results for SG09-SG012, which are located further away from the connection showed the strain values below the yielding strain. This reflects no trace of local buckling failure in the beam up to a large rotation, as evidenced in Fig. 11, corresponding to point C in Fig. 9. The strain values for all the sets of strain gauges at the beam flanges of the SRC-S-4 specimen, on the other hand, exceeded yielding strain and dropped at around θ= 0.05-0.06 rad, corresponding to point C in Fig. 12. This reflects the occurrence of the web buckling as evidenced in Fig. 14.

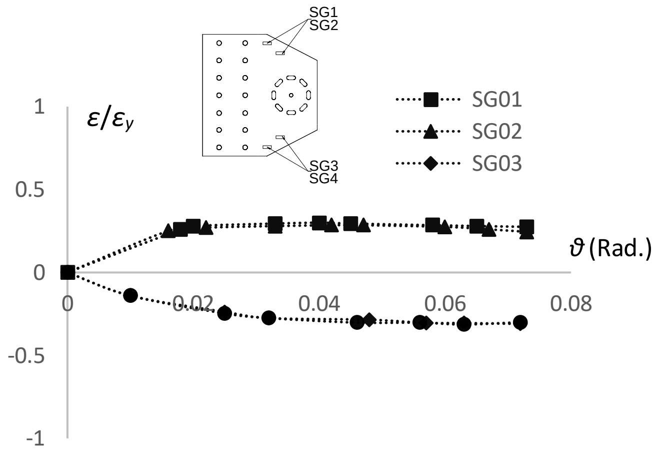

Fig 15. SC-S-4 TP maximum normalised strains (ε_y=0.2%) at each loading cycle.

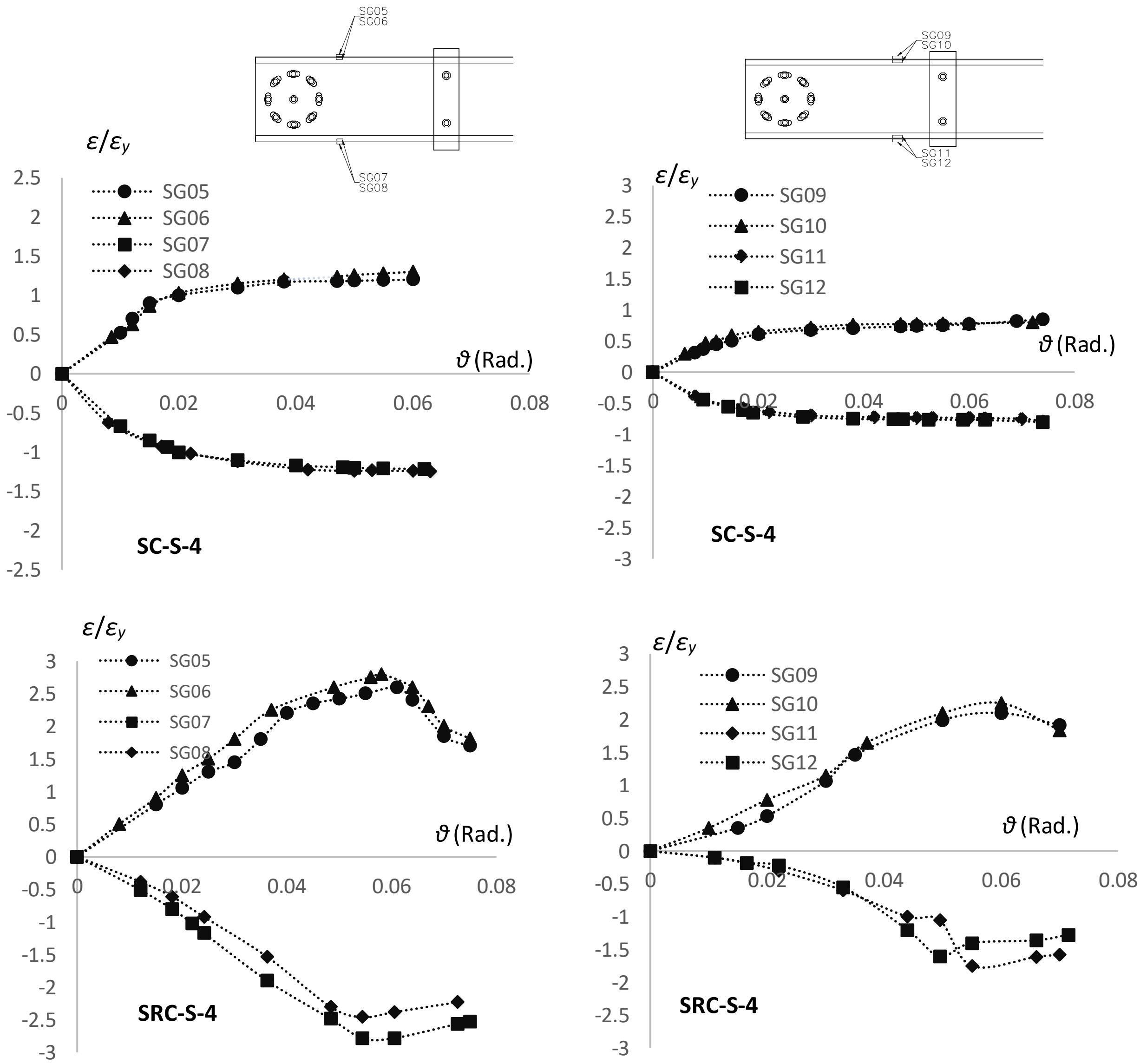

Fig 16. SC-S-4 and SRC-S-4 beam flanges maximum normalised strains (ε_y=0.2%) at each loading cycle.

5. General discussions

5.1. Energy dissipation

Fig. 17 shows the cumulative energy dissipation (E) for all the specimens derived from the areas surrounded by the hysteretic curves at 0.01 rad intervals up to θ = 0.06 rad. The SC specimens having either flat or segmental flange beams, shown by solid lines, dissipated a higher energy than that of the corresponding SRC specimens (identified by dashed lines) by 79%, 44% and 27%, respectively for connections with 2 mm, 4 mm and 6mm thickness beam at θ = 0.06 rad. This indicates the bolting friction-slip mechanism is more effective for connections with lower beam thicknesses which are typically more vulnerable to premature local and distortional buckling failures (see Fig. 13 for SRC-S-2 failures). Further, the SC specimens with segmental flange beams dissipated a higher energy by up to 26% compared with their flat flange beam counterparts which is due to the higher flange stiffness of the former type of beam sections.

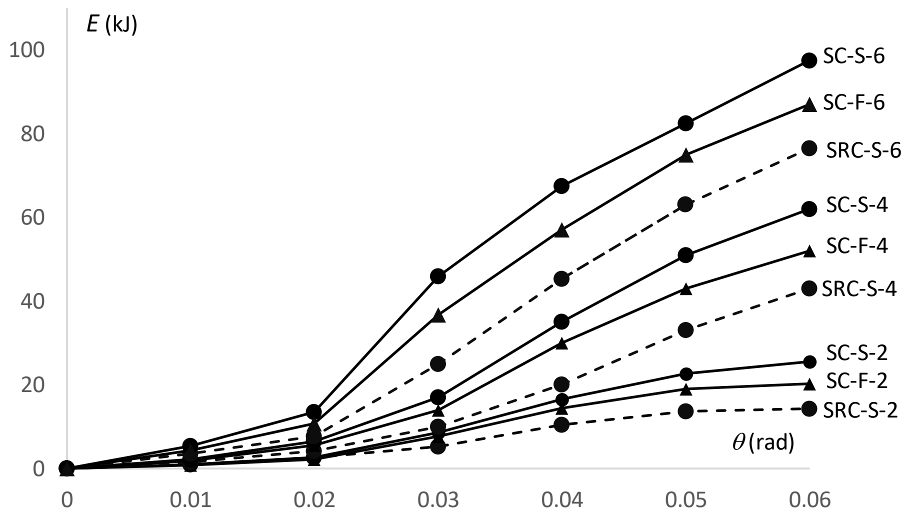

Fig 17. Cumulative energy dissipation (E) curves of all the SC and SRC specimens at each loading cycle.

5.2. Ductility capacity

To calculate the ductility capacity of the tested connections the FEMA bi-linear idealisation model [23] has been used (dotted lines in Fig. 18), based on which the yielding rotation, θ_y, can be determined. The ultimate rotation, θ_u, corresponds to the rotation at 80% of the post-peak moment determined based on the obtained backbone curves, shown by solid lines in Fig. 18 for the SC-S-2 and SRC-S-2 specimens. For the 4 mm and 6 mm SC and SRC specimens, with no or low strength degradation, θ_u was limited to 0.06 rad which is deemed a sufficiently large connection rotation in seismic performance of steel moment-frame structures (greater than 0.04 rad rotation required for SMFs [13]).

The ductility factor (μ) of the tested connections can then be calculated based on the ratio of $\mu = \theta_u / \theta_y$. The results for the calculated θ_y, θ_u and μ for all the tested connections are given in Table 4. The SC specimens produced a higher ductility than the corresponding SRC specimens by around 2.5 times for the connections with 2 mm and 4 mm beam thicknesses and 1.7 times for the connection with 6 mm thickness beam. This, again, reflects that the bolting friction-slip mechanism is more effective for connections with lower beam thicknesses. The ductility factors of the SC specimens having segmental and flat flanges are almost the same, revealing the dominance of the bolting slip on the connection behaviour. The exception being the connections with 2 mm thickness beam for which a higher level of ductility factor has been achieved for the connection with segmental flange beam than the connection with flat flange beam section.

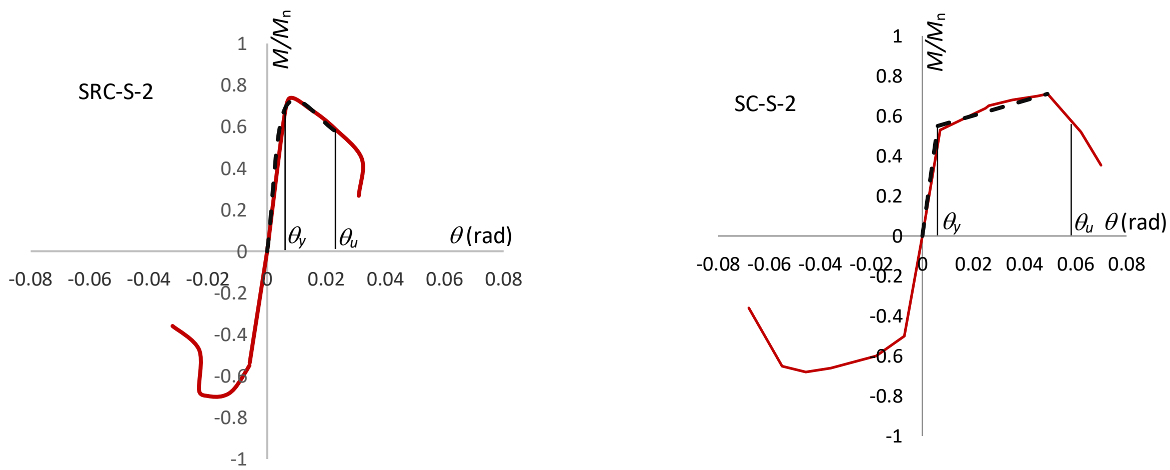

Fig 18. Bi-linear model constructed for the representative SC-S-2 and SRC-S-2 connections.

Table 4. Ductility factor of the tested connections.

Connection label	θ_y (rad)	θ_u (rad)	μ
SC-S-2	0.007	0.057	8.1
SC-F-2	0.0127	0.058	4.6
SRC-S-2	0.0075	0.024	3.2
SC-S-4	0.005	0.06	12
SC-F-4	0.005	0.06	12
SRC-S-4	0.013	0.06	4.6
SC-S-6	0.007	0.06	8.6
SC-F-6	0.007	0.06	8.6
SRC-S-6	0.012	0.06	5

6. Summary and Conclusion

Nine full-scale tests were conducted to investigate the effect of the slotted bolting friction-slip mechanism on cold-formed steel (CFS) beam-to-column connections. These involved both slip and slip-resistant connections (SC and SRC, respectively) having segmental (S) or flat (F) flange beam sections tested under cyclic loading for comparison purposes. A range of 2 mm, 4 mm and 6 mm beam thicknesses were tested. The obtained hysteretic curves showed that all the SC specimens satisfied the requirements of the Special Moment Frames (SMF) specified in the AISC Seismic Provisions, while the SRC specimen with 2 mm beam thickness experienced a sharp strength degradation due to a premature web local buckling. The SRC specimens with higher thicknesses of 4 mm and 6 mm, however, still satisfied the SMF requirements though affected by web local buckling at a relatively large rotation. The peak moment of connections with 2 mm beam thickness was in the range of 0.6-0.7 M_n, while the peak moment for the connections having 4 mm and 6 mm thicknesses reached around 0.8-1.0 M_n. As expected, the connections with segmental flange beams showed a relatively higher peak moment compared with their corresponding connections using flat flange beam sections.

It was also shown that the energy dissipation and ductility capacities of the SC specimens with 2 mm beam thickness were respectively 79% and 2.5 times higher than those of the corresponding SRC configurations, while these values were reduced to 27% and 1.7 times for the connections with 6 mm beam thickness. In general, the connections with the lower beam thicknesses benefitted more from the bolting friction-slip mechanism.

Incorporation of the obtained moment-rotation responses into the frame-level analysis could be a valuable investigation to be followed-up.

Acknowledgement

The tests reported herein were conducted at the Structures Laboratory of Building and Housing Research Centre of Iran with technical support from Iran Tohid Co. which are much appreciated. The first author is grateful to the Elphinstone PhD Scholarship provided by the University of Aberdeen.

References

[1] Robert L. Madsen Thomas A. Castle Benjamin W. Schafer (2016). Seismic Design of Cold-Formed Steel Lateral Load-Resisting Systems. NIST GCR 16-917-38. Applied Technology Council.

[2] Mohebbi, S., Mirghaderi, SR., Farahbod, F., Bagheri Sabbagh, A. & Torabian S. (2016). Experiments on seismic behaviour of steel sheathed cold-formed steel shear walls cladded by gypsum and fiber cement boards. Thin-walled Structures, 104, 238-247.

[3] Mohebbi S., Mirghaderi R., Bagheri Sabbagh A. (2015). Experimental work on single and double-sided steel sheathed cold-formed steel shear walls for seismic actions. Thin-Walled Structures, 91, 50-62.

[4] D. Ayhan, BW. Schafer (2019). Cold-formed steel ledger-framed construction floor-to-wall connection behaviour and strength. Journal of Constructional Steel Research. 156, 215-226.

[5] A. Bagheri Sabbagh, S. Torabian (2021). "Semi-rigid floor-to-wall connections using side-framed lightweight steel structures: Concept development", Thin-Walled Structures, 160,107345.

[6] Uang C-M, Sato A., Hong J-K, Wood K. (2010). Cyclic testing and modeling of cold-formed steel special bolted moment frame connections, Journal of Structural Engineering, Vol. 136, No. 8, 953-960.

[7] Sato A., Uang C-M (2009). Seismic design procedure development for cold-formed steel–special bolted moment frames. Journal of Constructional Steel Research, 65,860–868.

[8] ANSI-AISI-S400-15. North American Standard for Seismic Design of Cold-Formed Steel Structural Systems. Washington, D.C.: American Iron and Steel Institute.

[9] Bagheri Sabbagh A., Petkovski M., Pilakoutas K., Mirghaderi R. (2011). Ductile moment-resisting frames using cold-formed steel sections: An analytical investigation. Journal of Constructional Steel Research, 634–646.

[10] Bagheri Sabbagh A., Petkovski M., Pilakoutas K., Mirghaderi R. (2012). Development of cold-formed steel elements for earthquake resistant moment frame buildings, Thin-Walled Structures, 53, 99–108.

[11] Bagheri Sabbagh A., Petkovski M., Pilakoutas K., Mirghaderi R. (2012). Experimental work on cold-formed steel elements for earthquake resilient moment frame buildings. Engineering Structures, 42, 371–386.

[12] Bagheri Sabbagh A., Petkovski M., Pilakoutas K., Mirghaderi R. (2013). Cyclic behaviour of bolted cold-formed steel moment connections: FEM including slip, Journal of Constructional Steel Research, 80, 100–108.

[13] ANSI/AISC 341-05 (2016), seismic provisions for structural steel buildings, American institute of steel construction (AISC), Illinois.

[14] CASCIATI F., DOMANESCHI M. (2007). Semi-active Electro-inductive Devices: Characterization and Modelling", Journal of Vibration and Control 2007, 13(6):815-838.

[15] Ye J., Mojtabaei S.M., Hajirasouliha I., Shepherd P. (2019). Seismic performance of cold-formed steel bolted moment connections with bolting friction-slip mechanism, Journal of Constructional Steel Research, 156, 122-136.

[16] A. Bagheri Sabbagh, N.Jafarifar, D. Denyz, S. Torabian (2022). "Development of Composite Cold-Formed Steel-Rubberised Concrete Semi-Rigid Moment-Resisting Connections", Structures, 40, 866–879.

[17] Shahini M., Bagheri Sabbagh A., Davidson P., Mirghaderi R. (2018). Cold-formed steel bolted moment-resisting connections with friction-slip mechanism for seismic areas. 24th International Specialty Conference on Cold-Formed Steel Structures (CCFSS, 2018), St. Louis, MO.

[18] Shahini M., Bagheri Sabbagh A., Davidson P., Mirghaderi R. (2019). Development of cold-formed steel moment-resisting connections with bolting friction-slip mechanism for seismic applications, Thin-Walled Structures, 53, 99–108.

[19] M. Shahini, G. Saedi, R. Mirghaderi (2017). Improving seismic performance of the non-structural light steel framing systems using sliding bolted connections, 39th IABS symposium, Vancouver, BC, Canada.

[20] AISI-S100-16. North American Specification for the Design of Cold-Formed Steel Structural Members. Washington, D.C.: American Iron and Steel Institute; 2016.

[21] Li Z, Schafer BW (2010) "Buckling analysis of cold-formed steel members with general boundary conditions using CUFSM: conventional and constrained finite strip methods." Proceedings of the 20th International Speciality Conference on Cold-Formed Steel Structures, St. Louis, MO.

[22] Eurocode 3: design of steel structures: Part 1.8: Design of joints, EN 1993-1-8; 2005.

[23] FEMA- 356, Pre standard and Commentary for the Seismic Rehabilitation of Buildings, American Society of Civil Engineers, USA, Virginia, 2000.